Quantification of the Synergetic Contribution of a Buried WO_3/TiO_2 Heterojunction to Photocatalytic Activity

C. Sotelo-Vazquez,[1,2] R. Wilson,[3] R. Lee,[4] M. Ling,[3] S. Sathasivam,[5,6] R. Palgrave,[3] C.S. Blackman,[3] I.P. Parkin,[3] A. Iqbal,[7]* A. Kafizas[8]* and R. Quesada-Cabrera.[3,9]*

[1] Chemical and Environmental Engineering Group, ESCET, Universidad Rey Juan Carlos, C/Tulipán s/n, Móstoles, Madrid 28933, Spain.

[2] Instituto de Investigación de Tecnologías para la Sostenibilidad, Universidad Rey Juan Carlos, C/Tulipán s/n, Móstoles, Madrid 28933, Spain.

[3] Department of Chemistry, UCL (University College London), 20 Gordon St, London WC1H 0AJ, United Kingdom.

[4] Department of Energy Conversion and Storage, Technical University of Denmark, Fysikvej, 2800 Kgs. Lyngby, Denmark.

[5] School of Engineering & Design, London South Bank University, 103 Borough Road, London SE1 0AA, United Kingdom

[6] Energy, Materials & Environment Research Centre, London South Bank University, 103 Borough Road, London SE1 0AA, United Kingdom

[7] Materials Engineering, McGill University, 3610 University Street, Montréal QC H3A0C5, Canada.

[8] Department of Chemistry, Imperial College London, The Molecular Science Research Hub, 82 Wood Lane, White City, London W12 0BZ, United Kingdom.

[9] Department of Chemistry, FEAM-iUNAT, Universidad de Las Palmas de Gran Canaria, Campus de Tafira 35017, Las Palmas de Gran Canaria, Spain.

Email: raul.quesada@ulpgc.es ; a.kafizas@imperial.ac.uk ; asif.iqbal@mail.mcgill.ca

Supplementary Information

Table of Contents

1. Film Growth and Characterisation

A schematic figure of the CVD apparatus used in this work is shown in **Fig. S1**. In the aerosol-assisted (AA)CVD synthesis, we used a precursor solution containing tungsten hexacarbonyl ($W(CO)_6$ 1.14 $\times 10^{-2}$ M) in a 2:1 mixture of acetone and methanol under ultrasonic conditions (2 MHz). The CVD reactor was set at a temperature of 350°C ± 10°C. In the atmospheric-pressure (AP)CVD synthesis, bubbler temperatures were set at temperatures to generate enough vapour pressure for the precursors (*i.e.* 70 °C and 40 °C for titanium tetrachloride, $TiCl_4$ and ethyl acetate, $C_4H_8O_2$, respectively). Argon or nitrogen gas are typically used as carrier gases. Gas flow rates were 1.2 L min^{-1} and 0.25 L min^{-1}, respectively for $TiCl_4$ and $C_4H_8O_2$. The precursors were pre-mixed in a mixing chamber before entering the CVD reactor. The deposition temperature was set to 500 °C.

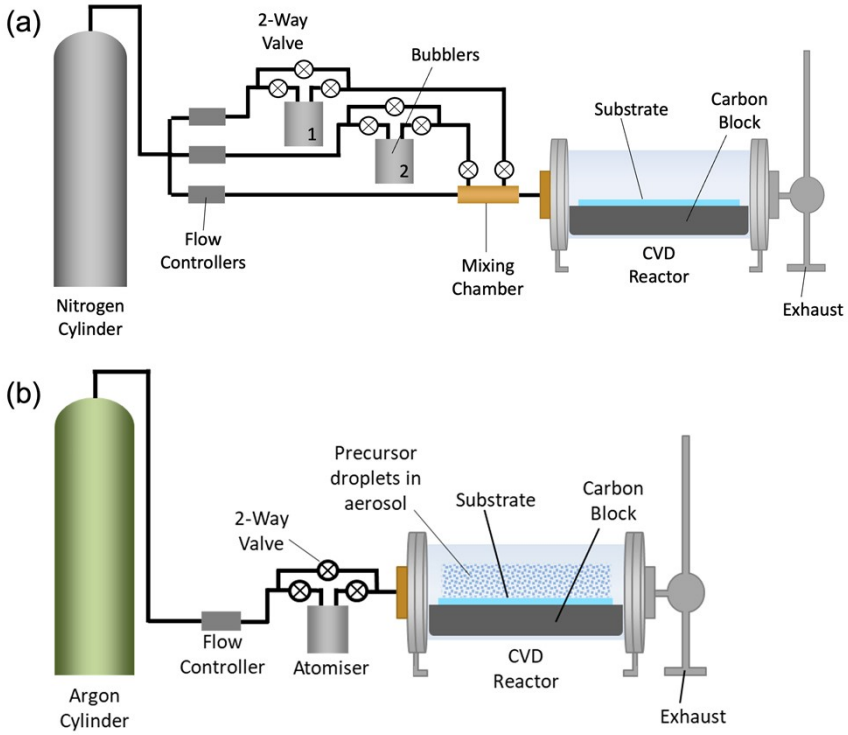

Fig S1. Schematic figure of the (a) AACVD used for the synthesis of WO_3 nanorods and (b) APCVD systems used for the synthesis of TiO_2 coatings.

During the CVD synthesis, a *conformal growth regime,* t_{CG} (**Fig. S2**) was established within deposition times between 15-60 s, with a constant rate of *ca*. 1.7 nm s^{-1}. Below this regime (t < 15 s), the samples consisted of TiO_2-supported WO_3 nanorods, whereas long deposition times (t > 60 s) resulted in the coalescence of TiO_2 film growth between neighbouring WO_3 nanorods, causing the nanorods to become embedded within the TiO_2 coating, and is herein deemed non-conformal (*i.e. nc*-WTi). Film thicknesses were measured from TEM analysis, with selected images as given in Fig. 1, and they were also estimated from EDS analysis (**Fig. S3**).

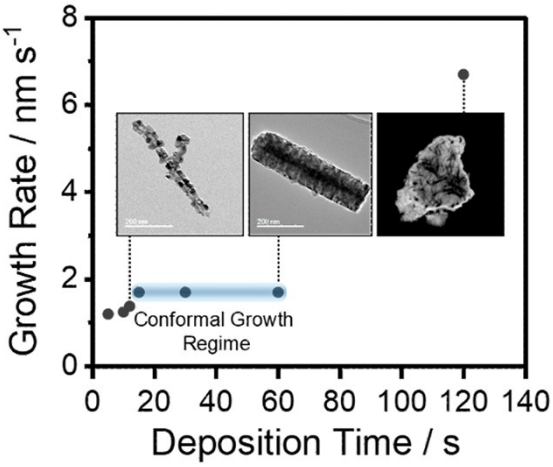

Fig S2. Growth rates for the deposition of TiO_2 coatings by CVD on WO_3 nanorods, highlighting the conformal growth regime (t_{CG}) observed within short deposition times under the synthesis conditions employed in this work. SEM images of corresponding deposition times are included for reference.

In the ALD synthesis, the TiO_2 coatings were deposited from titanium (IV) isopropoxide (TTIP, $Ti[OCH(CH_3)_2]_4$) and water (H_2O), using nitrogen as carrier gas. The bubbler temperatures were set to 25°C and 5°C under gas flow rates of 50 sccm and 0 sccm, respectively. Dose and purge times for TTIP were 2.5 s and 60 s, respectively. Dose and purge times for water were 2 s and 180 s, respectively. Purge lines were set to 50 sccm. The deposition temperature for the ALD TiO_2 films was set to 200 °C. Examples of specific deposition conditions for selected films are given in **Table S1**. These conditions were explored from deposition of pure TiO_2 films on quartz substrates (**Fig. S4**).

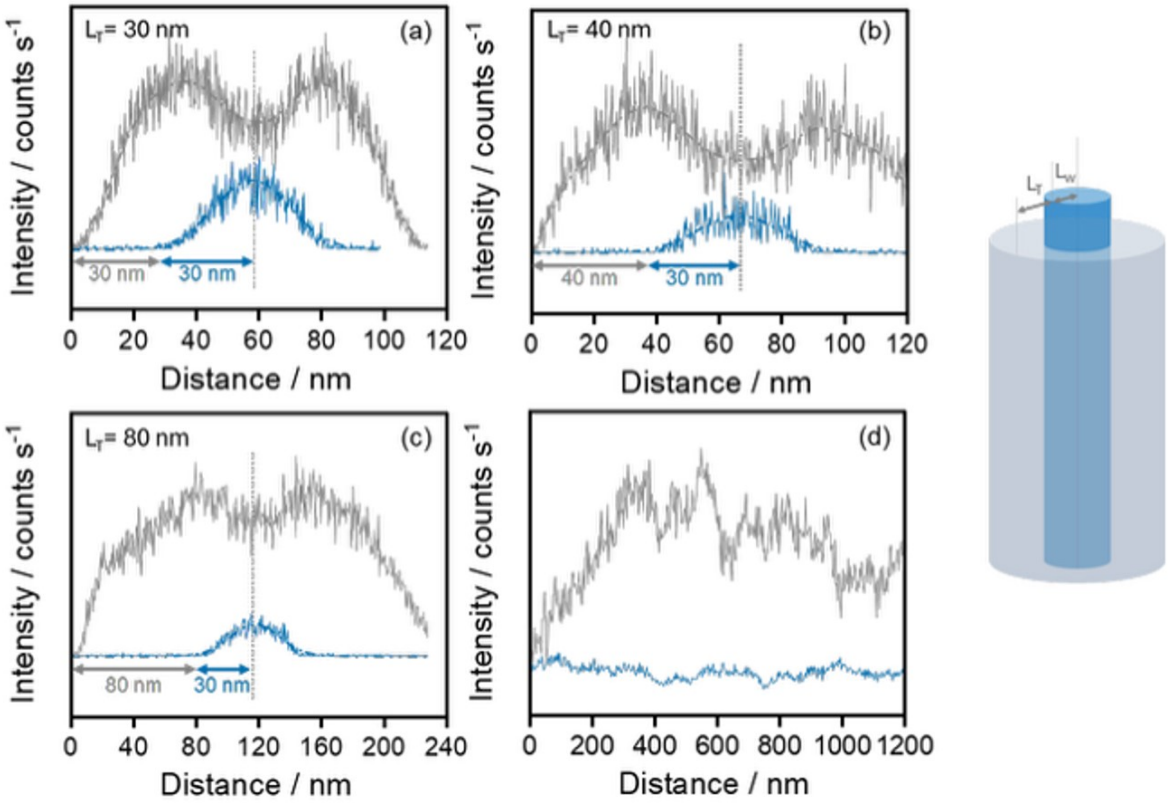

Fig S3. Elemental analysis (EDS) curves tracing titanium (Ti, grey lines) and tungsten (W, blue lines) in heterojunction WTi films deposited from CVD methods. Average radii values for WO_3 (L_w= 30 nm) and TiO_2 L_T values, respectively (a) 30, (b) 40, and (c) 80 nm are indicated. (d) EDS results from a conventional (i.e. non-conformal) nc-WTi film, with WO_3 nanorods embedded into a TiO_2 film, was included for comparison.

Table S1. ALD conditions given by the number of cycles, growth (Å/cycle) and running pressure, P_R (mbar), used in the deposition of TiO_2 coatings (average radial thicknesses, L_T, in nm) on WO_3 nanorods.

#	cycles	P_R (mbar)	Growth (Å/cycle)	L_T (nm)
WTi-3	120	1.13	0.22	3
WTi-9	225	1.26	0.41	9
WTi-13	300	1.31	0.42	13
WTi-21	650	1.83	0.32	21
WTi-65	1100	1.35	0.64	65
WTi-110	1865	1.35	0.59	110

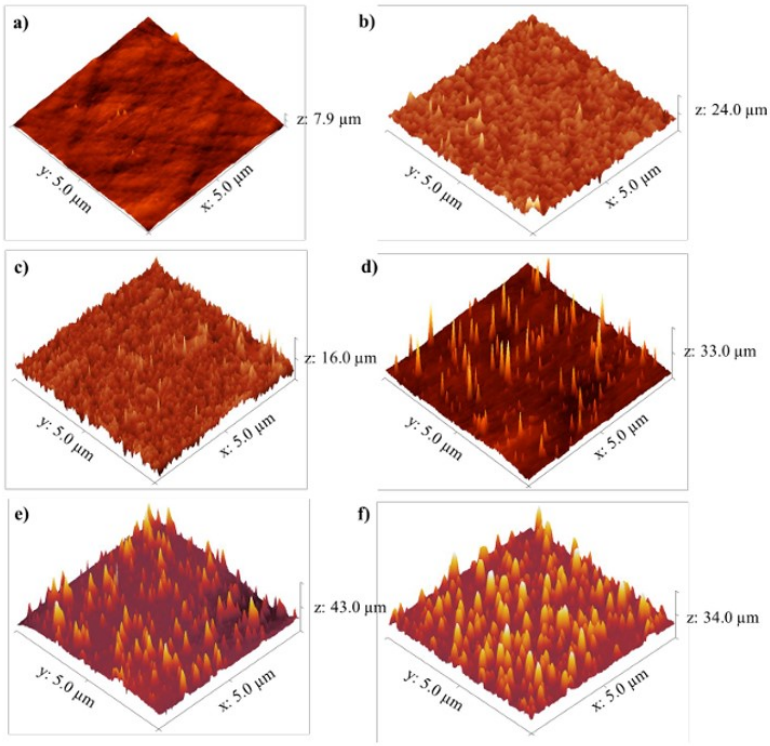

Fig S4. AFM images of TiO_2 films deposited on quartz substrates at 200 °C over (a) 100 cycles, (b) 400 cycles, (c) 600 cycles, (d) 800 cycles, (e) 1200 cycles and (f) 1500 cycles. Images set to a physical scale factor of 50 in the z axis (adapted from R.L. Wilson, PhD thesis, UCL (University College London)).

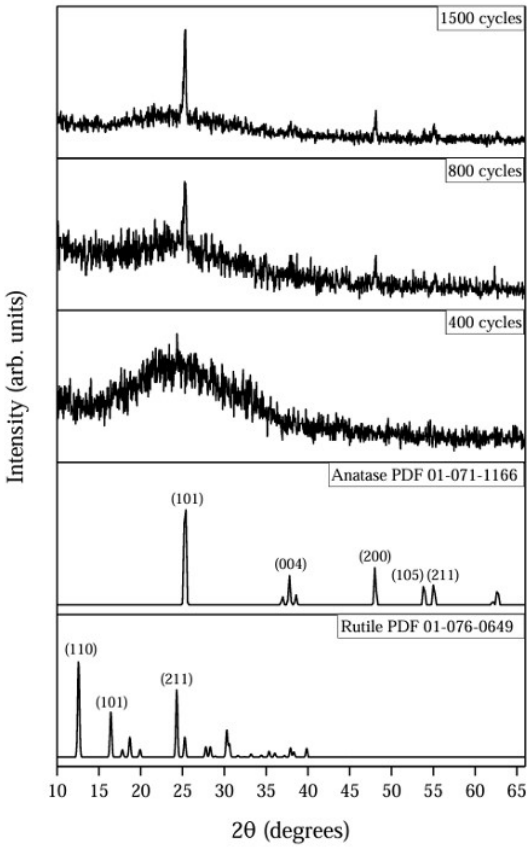

Fig S5. XRD analysis of selected TiO_2 films deposited using ALD on glass substrates after 400, 800 and 1500 cycles, resulting in film thicknesses of 10, 38 and 80 nm, respectively.

The presence of monoclinic WO_3 and anatase TiO_2 phases was confirmed from XRD and Raman spectroscopy analysis (**Fig. 2**). Le Bail refinement (**Table S2**) showed negligible changes in unit cell volume and average crystal size for either phase (**Fig. S6a,b**) when compared with powder standards, which rules out metal ion diffusion between the two oxide lattices. The Raman spectra were dominated by anatase TiO_2 characteristic bands with additional weak bands assigned to monoclinic WO_3 (**Fig. 2b**). The main band in anatase TiO_2 (E_g mode) (**Fig. S6c**), attributed to symmetric O-Ti-O stretching vibrations, remained at 141 cm^{-1} across all the samples, which further confirmed the integrity of the TiO_2 phase and absence of metal ion diffusion.

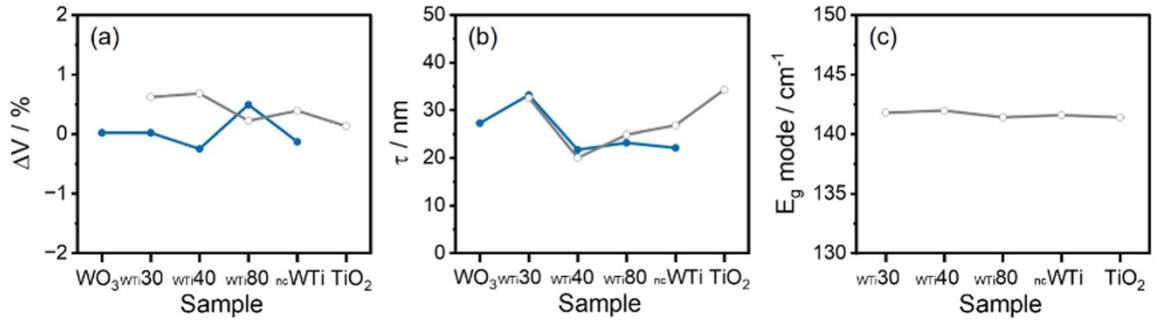

Fig S6. (a) Percentage of unit cell volume change, respectively, WO_3 (blue line) and TiO_2 (grey line), in CVD WTi heterojunction films and parent materials. (b) Corresponding average crystallite length scales for the same samples. (c) Raman shift for the characteristic E_g mode (141.8 cm^{-1}) in anatase TiO_2.

Table S2. Unit cell lattice parameters derived from Le Bail refinement of XRD data from monoclinic (m) WO_3 and anatase (a) TiO_2 phases, respectively. W_{Rp} is the weighed residual of least-squares refinement and ΔV(%) is the lattice volume expansion relative to a powder standard. Average crystallite size, τ is given in nm.

	Phase	a	b	c	β	V	ΔV%	W_{Rp}	τ (nm)
Standards	a	3.7848	3.7848	9.5124	-	136.3	-	-	-
	m	7.3008	7.5389	7.6896	90.892	423.2	-	-	-
TiO_2	a	3.7847	3.7847	9.5249	-	136.4	0.13	0.164	32.6
WO_3	m	7.2874	7.5384	7.7010	90.781	423.0	-0.04	0.125	27.3
WTi-30	a	3.7935	3.7935	9.5277	-	137.1	0.62	0.093	20.0
	m	7.3127	7.5328	7.6844	90.61	423.2	0.02		33.2
WTi-40	a	3.7922	3.7922	9.5402	-	137.2	0.68	0.092	24.8
	m	7.2542	7.5381	7.7208	90.893	422.1	-0.25		21.7
WTi-80	a	3.7884	3.7884	9.5151	-	136.6	0.22	0.117	26.8
	m	7.3008	7.5564	7.7097	90.877	425.3	0.49		23.2
nc-WTi	a	3.7906	3.7906	9.5201	-	136.8	0.39	0.132	34.3
	m	7.2645	7.5489	7.7087	91.055	422.6	-0.13		22.1

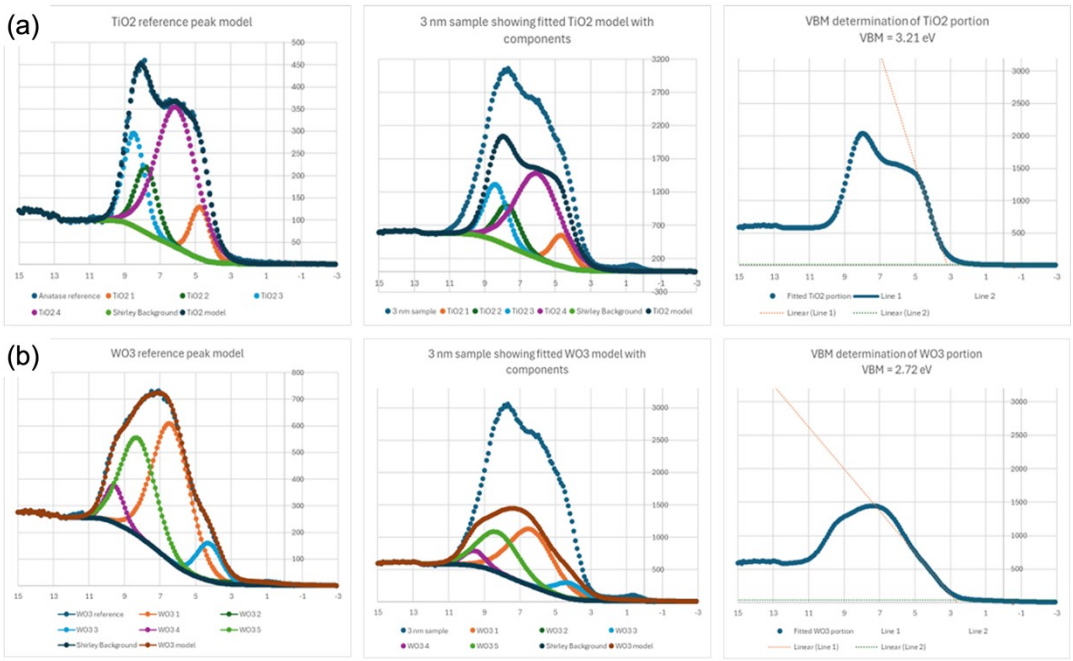

Fig. S7. Valence band (VB) spectra and peak models of (a) TiO_2 and (b) WO_3 including, from left to right, reference parent material, WTi-3 sample fitted with model and corresponding VB maxima.

2. Photocatalytic Properties

The photocatalytic activity of the WTi films was evaluated following the photodegradation of stearic acid during 2 h under UVA irradiation (λ= 365 nm, 2×8 W, *I*= 3.15 mW cm^{-2}). A thin layer of the acid was dip-coated onto the films from a chloroform solution (0.05 M). The photo-oxidation reaction (**Eq. S1**) was monitored from integrated areas of characteristic *C-H* bands at 2958, 2923 and 2858 cm^{-1} (**Fig. S8a**). Activity rates were estimated from linear regression of the curves of integrated areas as a function of irradiation time within a region of zero-order kinetics (**Fig. S8b**). The number of acid molecules degraded were estimated using the conversion factor 1 cm^{-1}≡ 9.7×10^{15} molecule cm^{-2} from the literature.[1] The full breakdown of one molecule of stearic acid involves 104 electron transfers.[2]

$$CH_3(CH_2)_{16}COOH + 26O_2 \rightarrow 18CO_2 + 18H_2O \qquad \text{(S1)}$$

The photocatalytic efficiency is evaluated in terms of the formal quantum efficiency, ξ, given as the number of molecules oxidised per incident photon. In this estimation, it is assumed that all incident photons have the same energy (*i.e. E*= 3.40 eV, λ= 365 nm). The photostability of the WTi films was demonstrated during cycling experiments over the course of 12 months (**Fig. S8c**).

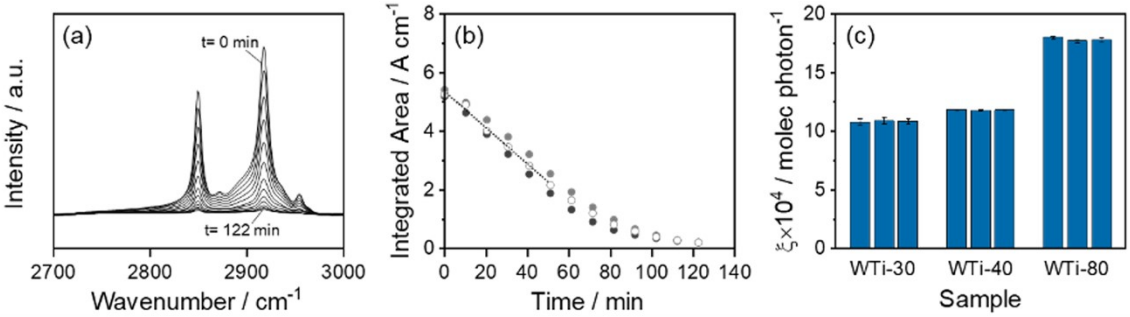

Fig S8. (a) Fourier-transform infrared spectroscopy analysis showing characteristic C-H bands of stearic acid on the WTi film surface under UVA irradiation. (b) Corresponding integrated areas of IR bands within 2700-3000 cm^{-1} as a function of irradiation time (2 h). (c) Reproducibility tests carried out after deposition of CVD samples (grouped from left to right, 0, 6 and 12 months after deposition).

3. Light Absorption Model

The degree of light absorption at 365 nm in a single nanorod was determined using a simple model. This was conducted at 365 nm as this was the wavelength of light used in our photocatalysis experiments. The model assumes that light hits the rod on its side, where we take the average situation where light hits the rod at its centre (**Fig. S9**). Given the random orientation of the nanorods, as evidenced by side-on SEM imaging (**Fig. 1a**), we assumed that the average angle of incidence of light upon each nanorod would be at 45°. Also, from TEM imaging, the average nanorod was assumed to be ~60 nm wide (**Fig. 1b**). This would mean that the average light path through each nanorod is:

$$60 \text{ nm} / \cos(45°) = 84.9 \text{ nm} \quad \text{(S2)}$$

With knowledge of the absorption coefficient of WO_3 (~102,400 cm^{-1}) [3] and TiO_2 (~9,900 cm^{-1}) [4] for 365 nm light, and thickness of each TiO_2 layer, we determined the degree of light absorption (%) as it transversed through a nanorod using the Beer-Lambert Law:

$$\text{Transmission (\%)} = e^{-\alpha l} \times 100(\%) \quad \text{(S3)}$$

where α and l are the absorption coefficient (cm^{-1}) and thickness (cm) for a given material, respectively.

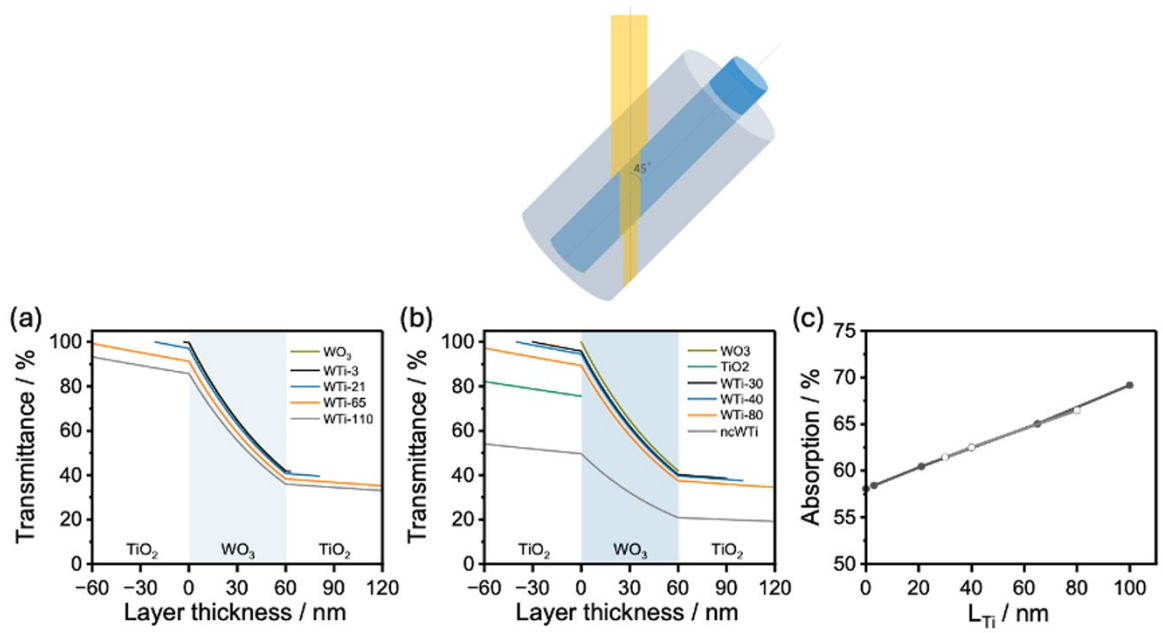

Fig S9. Schematic of our model of light absorption at 365 nm within a single nanorod, with incident light at 45° to the centre of the nanorod, for the series of WTi produced by (a) ALD and (b) CVD. (c) Total absorption (%) was found to change linearly with an increase in TiO_2 layer thickness (nm).

4. Transient Absorption Spectroscopy (TAS)

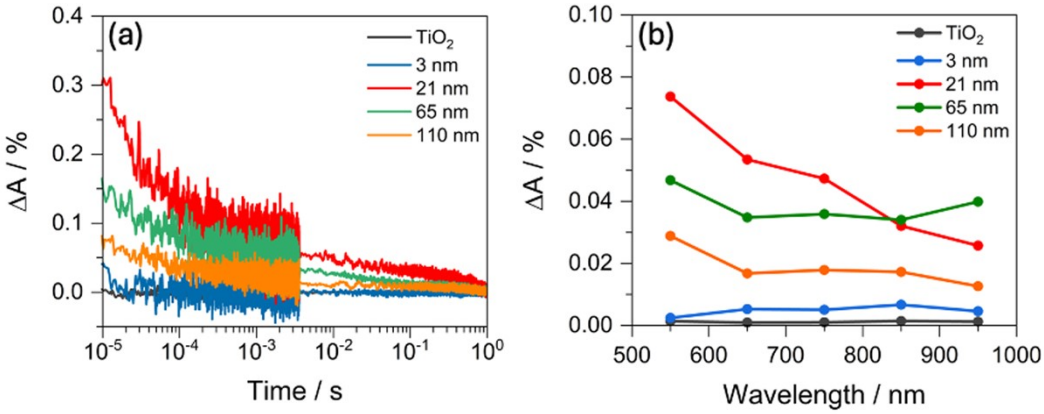

Fig. S10. Transient absorption spectroscopy of a series of ALD WTi films (λ_{exc} = 355 nm, ~1.2 mJ.cm^{-2} per pulse, 0.65 Hz repetition rate). (a) The recombination dynamics probed at 550 nm from 10 µs to 1 s after the laser pulse, and (b) the transient absorption spectra from 550 to 950 nm at 1 ms after the laser pulse. TAS data from a ~90 nm thick TiO_2 film grown by ALD is included for reference.

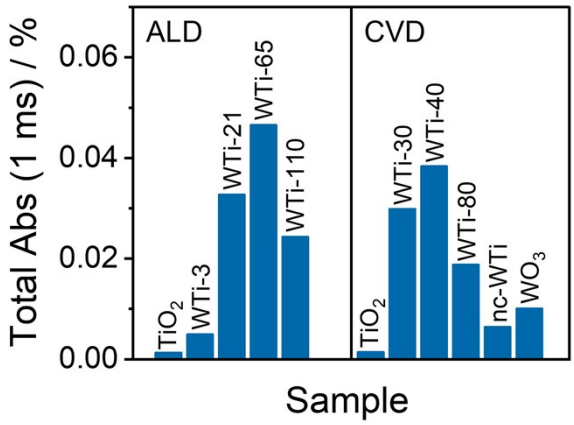

Fig. S11. Total transient absorption (from 550 – 950 nm, %) seen at 1 ms after the laser pulse (λ_{exc} = 355 nm, ~1.2 mJ.cm^{-2} per pulse, 0.65 Hz repetition rate) for both the ALD and CVD WTi series, alongside their parent materials, for a ~90 nm thick ALD TiO_2 and ~200 nm thick CVD TiO_2 film.

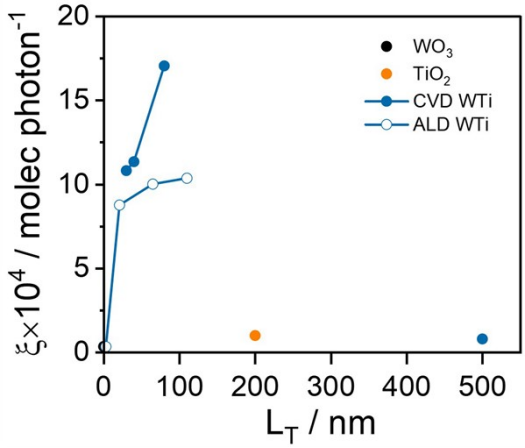

Fig. S12. A plot of the formal quantum efficiency (ξ, molecules degraded per photon) for the photocatalytic oxidation of stearic acid against TiO_2 coating thickness (L_T, nm) for both the ALD and CVD WTi series, plotted alongside WO_3 and TiO_2 (200 nm thick CVD TiO_2) parent materials for comparison.

5. Calculation Parameters

Table S3. Material parameters used in numerical computations.[5]

Material Parameters	Values
TiO_2 Bandgap Energy (eV)	3.2
TiO_2 Electron Affinity (eV)	5.1
TiO_2 Dielectric Constant	41.3
TiO_2 Electron Effective Mass	10
TiO_2 Hole Effective Mass	0.8
TiO_2 Bulk Electron Concentration (cm^{-3})	10^{18}
TiO_2 Absorption Co-efficient (cm^{-1})	9.9×10^3
WO_3 Bandgap Energy (eV)	2.74
WO_3 Electron Affinity (eV)	4.91
WO_3 Dielectric Constant	50
WO_3 Electron Effective Mass	2.4
WO_3 Hole Effective Mass	2.4
WO_3 Bulk Electron Concentration (cm^{-3})	10^{19}
WO_3 Absorption Co-efficient (cm^{-1})	1.02×10^5

References

[1] A. Mills and J. Wang, Simultaneous monitoring of the destruction of stearic acid and generation of carbon dioxide by self-cleaning semiconductor photocatalytic films, *J. Photochem. Photobiol. A. Chem*., 2006, **182**, 181-186.

[2] S. Alofi, C. O'Rourke and A. Mills, Study and Modeling of the Kinetics of the Photocatalytic Destruction of Stearic Acid Islands on TiO_2 Films, *J. Phys. Chem. C*, 2023, **127**, 12194-12205.

[3] A. Kafizas, L. Francas, C. Sotelo-Vazquez, M. Ling, Y. Li, E. Glover, L. McCafferty, C. Blackman, J. Darr and I.P. Parkin, Optimizing the Activity of Nanoneedle Structured WO_3 Photoanodes for Solar Water Splitting: Direct Synthesis via Chemical Vapor Deposition, *J. Phys. Chem. C*, 2017, **121**, 5983-5993.

[4] A. Kafizas, Y. Ma, E. Pastor, S.R. Pendlebury, C. Mesa, L. Francas, F. Le Formal, N. Noor, M. Ling, C. Sotelo-Vazquez, C.J. Carmalt, I.P. Parkin and J.R. Durrant, Water Oxidation Kinetics of Accumulated Holes on the Surface of a TiO_2 Photoanode: A Rate Law Analysis, *ACS Catal*., 2017, **7**, 4896-4903.

[5] A. Iqbal, A. Kafizas, C. Sotelo-Vazquez, R. Wilson, M. Ling, A. Taylor, C. Blackman, K. Bevan, I.P. Parkin, R. Quesada-Cabrera, Charge Transport Phenomena in Heterojunction Photocatalysts: The WO_3/TiO_2 System as an Archetypical Model, *ACS Appl. Mater. Inter*., 2021, **13**, 9781-9793.